Chemical Physics Letters 760 (2020) 137995

Contents lists available at ScienceDirect

Chemical Physics Letters

journal homepage: www.elsevier.com/locate/cplett

Research paper

Photoluminescence enhancement of perovskites nanocomposites using ion implanted silver nanoparticles

Shahid Iqbal [a,*], Masoud Shabaninezhad [a], Abubkr Abuhagr [b], Maryam Vaghefi [a], Guda Ramakrishna [b], Asghar Kayani [a]

[a] Department of Physics, Western Michigan University, Kalamazoo, MI 49008, USA
[b] Department of Chemistry, Western Michigan University, Kalamazoo, MI 49008, USA

ARTICLE INFO

Keywords:
Ion implantation
RBS
LSPR
Ag nanoparticles
Metal enhanced photoluminescence

ABSTRACT

Metal enhanced photoluminescence by 70 keV Ag ions implanted at various fluences in quartz substrates was studied using drop casted CsPbX (X = Br_3, I_3, BrI_2) perovskites. Concentration and depth profile of the implanted Ag was determined by Rutherford Backscattering Spectrometry. Ag nanoparticles existence was confirmed by optical absorption spectroscopy. Photoluminescence enhancement was obtained using steady state photoluminescence spectroscopy and enhancement was observed for $CsPbBrI_2$ and $CsPbI_3$ reaching as high as 3.6 and 5.9 fold, respectively. Whereas, a 60% photoluminescence quenching was observed for $CsPbBr_3$, which could be attributed to the non-radiative energy transfer from perovskite to nanoparticles.

1. Introduction

Localized surface plasmon resonance (LSPR) is a fundamental property of the plasmonic NPs that occurs when the frequency of the incident light matches the plasma frequency of the conduction electrons in metallic NPs [1–3]. This phenomenon produces a strong localized electric field around the plasmonic particles [4] and scatters and absorbs incident light [1,2,5,6]. LSPR frequency depends on parameters such as the size and shape of the NP, interparticle distance, the refractive index of the surrounding medium, the polarization direction of the incident light and the chemical ligands that surrounded them. [7–12] This property of the plasmonic NPs have attracted significant research interest in various applications including surface-enhanced Raman scattering (SERS), [13] Photoluminescence (PL) enhancement, [14,15] biosensing, [16–19] and biological imaging. [20,21] Interestingly, the LSPR properties of the plasmonic NPs can be used to modify the PL of metal halide perovskite crystals. [22,23] These nanocomposites have received significant attention because of the wide variety of optoelectronic applications including photovoltaics, [24,25] light-emitting diodes (LEDs), [26,27] amplified spontaneous emission lasing, [28,29] lasers, [30] and optical sensing [31]. Also, owing to their high performance, low cost, and abundance, these materials are considered the most promising materials for future optoelectronics [32].

Several studies were carried out to show the effect of chemically synthesized plasmonic nanostructures on the PL enhancement and quenching in perovskite nanocomposites [33–35]. For example, Xinyang Wu et al. reported fluorescence enhancement of $MAPbBr_3$ perovskites by doping metal nanoparticles into the PEDOT: PSS buffer layer [26]. They were able to successfully observe ~4-fold fluorescence enhancement of $CH_3NH_3PbBr_3$ perovskite. Pen Sun et al. have shown the PL study of perovskites ($CH_3NH_3PbI_3$) nanocrystals by using different metal films such as gold, silver, and aluminum using physical vapor deposition method. [36] They have used a spacer layer between the perovskites and film. This group observed 14-fold fluorescence enhancement for $CH_3NH_3PbI_3$ in the case of perovskite/Al_2O_3/treated-Al. [36] However, to the best of our knowledge, no study has been carried out on the PL enhancement and quenching properties of the nanocomposites using ion-implanted plasmonic NPs. There are advantages associated with the use of implanted plasmonic NPs to modify the PL of a material as compared to the NPs in solution [37–39]. One advantage is that the NPs are formed without any surface capping ligands. Moreover, using this method not only the direct interaction between the PL material and NPs can be avoided, but also the distance between them can be controlled via adjusting the energy of the ion beam [37–39].

The main objective of this study is to investigate Metal Enhanced Photoluminescence (MEP) of the perovskites in the close vicinity of ion-implanted Ag NPs. Ag NPs have been implanted within the quartz matrix

* Corresponding author.
E-mail address: shahid.iqbal@wmich.edu (S. Iqbal).

https://doi.org/10.1016/j.cplett.2020.137995
Received 17 June 2020; Received in revised form 8 September 2020; Accepted 9 September 2020
Available online 17 September 2020

using the ion implantation technique. The NPs synthesis in the quartz substrate was carried out by bombarding 70 keV Ag^- ions at different fluences. Colliding incident ions may change both the chemical and structural properties of the target. The structural modification depends on the type, energy and fluence of the ions beam, and substrate temperature [15,30,40–44]. In this study, UV/Visible measurements were used to confirm the existence of Ag NPs in quartz substrates. The concentration, composition and depth profile of the implanted Ag NPs was determined by the Rutherford Backscattering (RBS) technique and fitting the experimental and simulated data of RBS provided the depth profile of Ag NPs using the density of SiO_2. To understand the effect of the embedded Ag NPs on the PL of the perovskites, the PL of the $CsPbBrI_2$, $CsPbI_3$, and $CsPbBr_3$ perovskites nanocrystals were carried out using steady-state excitation and emission measurements. The PL depends on the distance between the perovskites and the implanted NPs as well as photonic mode density, which both can be controlled by the fluence of the incident ion beams [30]. The later effect depends on the size and interparticle distance between neighboring NPs, which leads to stronger electric field between and around the NPs due to LSPR effect. It has been observed that PL of the $CsPbBrI_2$ and $CsPbI_3$ enhances with increasing the fluence of the ion beams. On the other hand, the finding shows that the PL of $CsPbBr_3$ perovskites quenches with a consistent increase of the ion beam fluence.

2. Experimental section

2.1. Ion implanted sample preparation

Quartz matrix (SiO_2), 1 mm thickness and 5 mm in radius, were ion-implanted with the low energy Ag ions using the ion implantation technique. Ag ions were produced from the Source of Negative Ions by Cs Sputtering (SNICS II) that is connected to Western Michigan University's 6.0 MV Tandem Van de Graaff accelerator. The silver powder was compacted in the source cathode and placed in the source to produce negative Ag ions for ion implantation. The ion beam from the source was extracted, accelerated, and filtered by a 20° injection magnet and focused on the target sample holder that is placed on a LABVIEW controlled XY stage. The energy of the ions beam was selected by the Stopping and Range of Ions in Matter (SRIM) calculations, [32] and the negative Ag ions were implanted with the 70 keV beam energy at different ion fluences. The fluence of 1.1×10^{16}p/cm^2, 1.3×10^{16}p/cm^2, 3.0×10^{16}p /cm^2 and 4.5×10^{16}p/cm^2 were used for the implantation experiment. To obtain the concentration, composition, and depth distribution of implanted Ag NPs, RBS measurements were performed using He^{++} ions with the beam energy of 2.5 MeV. Backscattered helium particles were collected at 150° scattering, with the exit angle of 30°. The implanted Ag NPs within the quartz matrix were detected using optical absorption measurements. Details about the preparation of the substrate, RBS, and optical absorption analysis can be found in our previous work [15]. Also, halide perovksites were synthesized using the method described by Protesescu et al. [31]

2.2. Photoluminescence measurement

A 40 μL perovskites were drop casted on bare and silver implanted quartz substrates. Samples were kept at room temperature for about 45 min to dry before taking data. The steady state measurements were carried out using an Edinburgh F900 spectrofluorometer. Monochromators model M300 were used to select both the excitation and emission wavelengths. As sample compartment model UC920 were used for the target samples. A 450 W Xenon lamp was used as the excitation light source for collecting the PL emission and excitation spectra of the desired fluorophore materials and a single photon counting PMT model R918 P was used as the detector for steady-state measurements. The PL spectra of $CsPbBr_3$, $CsPbBrI_2$, and $CsPbI_3$ were monitored by excitation wavelengths of 420 nm, 480 nm, 570, and 620 nm. Slit widths for excitation and emission were fixed at 5 nm for all measurements and the resolution was fixed at 1 rev/min for all samples.

3. Results and discussion

The distance of implanted NPs from the surface of the substrate plays a crucial role in the PL study of the luminophores. Therefore, 70 keV energy of the Ag ions was selected using the SRIM calculation [32]. RBS measurements on the implanted substrates was carried out using 2.5 MeV He^{++} ions. Backscattered He ions were collected at 150° scattering with 30° exit angle. A representative plot of experimental and simulated RBS spectra of an Ag implanted in the quartz substrates is given in the Fig. 1. The simulation of the RBS experimental data was carried out using SIMNRA [33]. The Ag, Si, and O edges in the quartz substrate were at 2130 keV, 1480 keV, and 960 keV, respectively.

To simulate the RBS spectra, the implanted substrate was divided into three layers. The first layer had the elemental concentration matching the chemical composition of the quartz substrate (SiO_2), i.e., Si 34 at% and O 66 at%. The thickness of the first layer gives the depth at which Ag is implanted below the surface of the quartz substrate. The second layer was chosen as a mixture of Ag, Si, and O, and the third layer is the substrate (See Fig. 2). Using the bulk density of the quartz substrate (2.65 g/cm3) and the areal density of the first layer obtained by RBS, the thickness of the first layer was calculated and is shown in Table 1. The thickness of the first layer gives the depth of implanted silver particles below the quartz surface.

For RBS analysis, a depth scale in order of 10^{15} atoms/cm^2 (areal density) gives the number of the target atoms that are visible to the incident helium ion beam. Fig. 3 shows the RBS spectra of all Ag-implanted substrates at different fluences. It is observed that with increasing ion fluence, the peak intensities of Ag increases, indicating increased implanted fluence. Moreover, the front edge of the Ag peak is moving towards higher backscattered energy, which means depth below the surface, where Ag stops decreases. Previous studies have reported that low fluence ions after striking the substrate are dispersed throughout the stopping layer and are well separated from each other [34,35,37]. However, at higher fluences, Ag atoms will be closer to each other, resulting in a higher nucleation rate and consequently leading to forming nanoparticles [34,35,37]. We observed, that formation of nanoparticles within the quartz substrate takes place while implantation process is being carried out. With the increase in fluence, nucleation rate increases, which reduces the projected range of the implanted Ag, therefore, newly formed nanoparticles nucleate closer to the surface of the substrates [30,35] Moreover, with the increase in the fluence, the

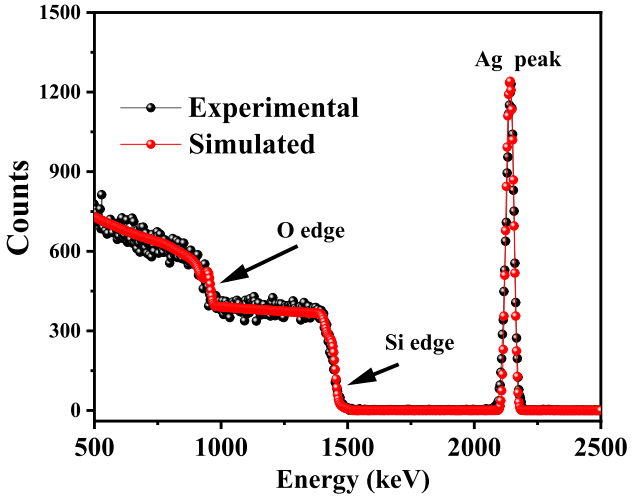

Fig. 1. Experimental and simulated RBS plots for the Ag-Implanted quartz substrate with ion beam fluence of 4.5×10^{16}p/cm^2.

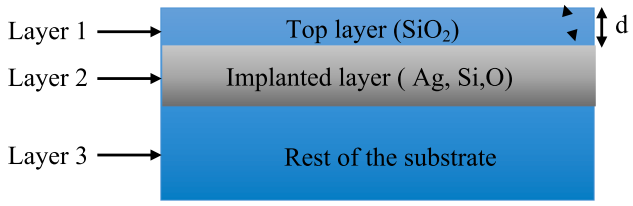

Fig. 2. Schematic diagram of the three layers ion-implanted structure.

Table 1
Calculated thickness of the first layer of Ag implanted quartz with respect to different fluences.

RBS fluence(p/cm^2)	Areal density (atoms/cm^2)	Thickness (nm)
1.1×10^{16}	24×10^{16}	30
1.3×10^{16}	21×10^{16}	26
3.0×10^{16}	17×10^{16}	23
4.5×10^{16}	9×10^{16}	12

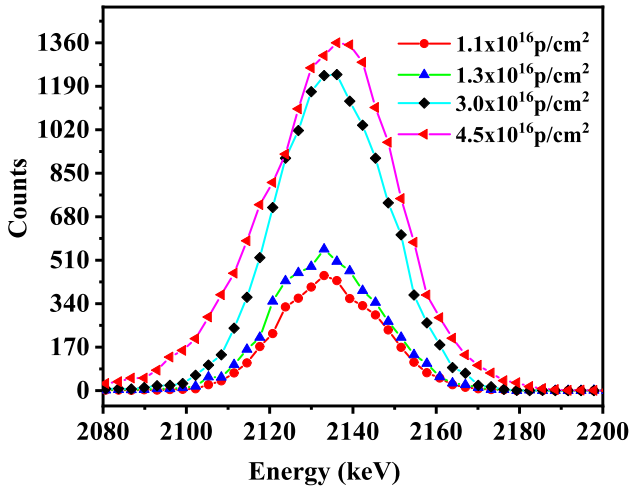

Fig. 3. Overlapped experimental RBS spectra for backscattered He ions between 2100 and 2226 keV showing the peak intensity increases with fluence for Ag implanted in quartz substrates.

size of the NPs increases that bring Ag NPs closer to the surface as well.

Using the bulk density of the quartz substrate (2.65 g/cm^3) and the areal density of the first layer obtained by RBS, the thickness of the first layer was calculated and is shown in Table 1. The thickness of the first layer gives the depth of implanted silver particles below the quartz surface.

To confirm the formation of Ag NPs within the quartz substrate, we used optical absorption spectroscopy. The absorption spectra of Ag implanted substrates at different ion beam fluences are given in Fig. 4. The characteristic LSPR peak is observed in all the spectra confirming the formation of NPs. Fig. 4 shows that by increasing the ion beam fluence, the LSPR absorption peak increases and broadens. This indicates that the number and the size distribution of NPs within the substrates increases with increasing fluence. Moreover, LSPR peak shifts from 396 nm to 414 nm for substrates implanted with 1.1×10^{16}p/cm^2 and 4.5×10^{16}p/cm^2, respectively. This could be associated to the average increase in the size of NPs and decreasing inter-particle distances that enhance inter-particle coupling effect (formation of hot-spots). The same behavior of absorption spectra was shown in our previous report [15].

The average size distribution of the implanted Ag NPs in the quartz substrate has been calculated in our previous study [15]. We considered spherical shape for the NPs, and the absorption spectra of the Ag NPs

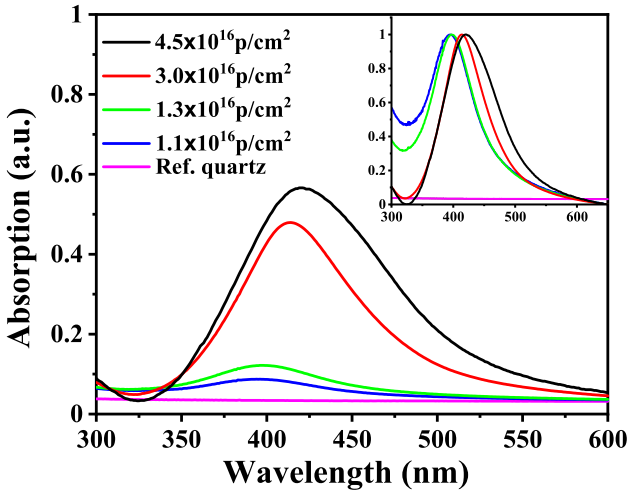

Fig. 4. Absorption spectra of the quartz substrates implanted with Ag NPs at different fluences. The inset shows the normalized plot, clearly depicting a red shift of the LSPR peak. (For interpretation of the references to colour in this figure legend, the reader is referred to the web version of this article.)

with diameters from 1 to 15 nm were calculated using Mie theory [45]. Then, the average diameter of the implanted NPs in each sample has been obtained by the composition-weighted average. This is in agreement with experimental data, the theoretical results in our previous work [15] have shown that the average size of the implanted NPs increases with enhancing the fluence. For example, the average diameter of the NPs increases from 2.2 nm to 5.6 nm as the fluence of the Ag ions enhances the fluence from 1.1×10^{16}p/cm^2 to 3.0×10^{16}p/cm^2

To investigate the effect of implanted Ag NPs on the PL properties of adsorbed perovskite nanocomposites CsPbX (X = Br_3, I_3, and BrI_2), first, the absorption spectra of the CsPbX on bare quartz and on Ag-implanted quartz were taken. The absorption spectra of Ag implanted quartz were then subtracted from the spectra of CsPbX on Ag implanted quartz. The result was then compared with the spectra of CsPbX on bare quartz. The comparison gave us no significant difference, which means that there is no direct interaction between adsorbed CsPbX and implanted NPs. The representative plot of the process explained above for $CsPbBr_3$ perovskite is given in Fig. 5.

Steady-state PL measurements were carried out for the adsorbed

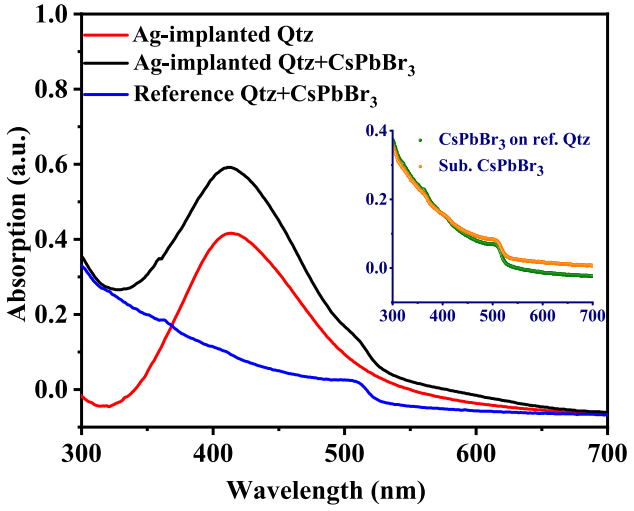

Fig. 5. Absorption spectra of the Ag-implanted substrate, Ag-implanted substrate with the $CsPbBr_3$, and reference substrate with the $CsPbBr_3$. The inset represents the comparison between the subtracted $CsPbBr_3$ with the $CsPbBr_3$ on the reference substrate.

CsPbX on bare and Ag implanted quartz to investigate the effect of implanted Ag NPs on PL properties of CsPbX. Moreover, it has been reported that the PL enhancement is significant if the excitation wavelength in steady-state measurement is chosen to be closer to the LSPR wavelength of the NPs. [38,39] Therefore, we used the excitation wavelength of 420 nm (on-resonance), and wavelength within LSPR and the emission of CsPbX.

We observed the PL enhancement for $CsPbBrI_2$ (Fig. 6.) and $CsPbI_3$ (Fig. 7.) on the Ag-implanted quartz as compared to the bare quartz substrate. Moreover, we observed the subsequent enhancement for $CsPbBrI_2$ and $CsPbI_3$ on the substrates implanted with higher Ag fluence. The observed enhancement of the PL intensity can be attributed to the enhanced electric field due to the LSPR of plasmonic Ag NPs within the quartz matrix. LSPR of the Ag NPs increases the excitation cross-section of the perovskite due to the localized enhanced electric field of excited Ag NPs. Consequently, the PL intensity of the perovskite is enhanced. With the increase of Ag ion fluence, the size and number of the NPs increase, leading to a reduced inter-particle gap resulting in the coupling between plasmons of the neighboring NPs. Moreover, RBS data suggests that the substrates implanted with higher fluence brings NPs closer to the surface, which reduces the distance between NPs and the adsorbed molecules. This further increases the excitation cross-section of the molecule resulting in more PL enhancement.

As mentioned before, we excited the perovskites at two different excitation wavelengths, one was chosen to be close to LSPR wavelength of the implanted Ag NPs, and the other one was selected to be off resonance. Fig. 6 (a) and 7 (a) show that there has been a significant increase in the PL enhancement for $CsPbBrI_2$ and $CsPbI_3$ at the excitation wavelength of 420 nm (on-resonance). Note from Table 2, the PL intensity of the $CsPbBrI_2$ perovskite increased by 260% and 62% at the excitation wavelength of 420 and 570 nm, respectively. Also, in the case of $CsPbI_3$, 490% PL enhancement was observed at the excitation wavelength of 420 nm, whereas this factor reduced to 180% when the excitation wavelength was chosen to be 620 nm. Exciting the samples with a wavelength close to the LSPR peak of the implanted Ag NPs significantly enhances the electric field around the NPs, which increases the excitation cross-section of the perovskite. However, when the excitation wavelength away from the LSPR peak is used, the electric enhancement around the NPs will be less, resulting in less PL enhancement. Our result is in agreement with the literature. [38,46,47]

On the other hand, for $CsPbBr_3$ adsorbed on Ag implanted quartz, we observed PL quenching at both on and off-resonance excitation wavelengths. Quenching factor increased for $CsPbBr_3$ on the substrates implanted with higher fluence, as shown in Fig. 8. In the case of PL quenching, negligible dependence on excitation wavelength was observed. PL intensity of the $CsPbBr_3$ excited by on resonance wavelength dropped by 27% on substrate implanted at 1.1×10^{16}p/cm^2 and by 60% on substrate implanted with the fluence of 4.5×10^{16}p/cm^2. However, the PL intensity of the $CsPbBr_3$ excited by off-resonance wavelength dropped by 26% on substrate implanted at 1.1×10^{16}p/cm^2 and by 54% on substrate implanted with the fluence of 4.5×10^{16}p/cm^2. The quenching of the PL intensity of the $CsPbBr_3$ can be attributed to the non-radiative energy transfer from $CsPbBr_3$ perovskite to Ag NPs.

The observed enhancement in $CsPbBrI_2$ and $CsPbI_3$ and quenching in $CsPbBr_3$ can be explained by plotting the normalized Ag NPs absorption and CsPbX emission spectra, as shown in Fig. 9. Our results show that the spectral overlap of the emission spectra of perovskite nanocomposites and the absorption spectra of ion implanted Ag NPs dictates the PL enhancement or quenching.

It can be seen from Fig. 9, that the emission spectra of the $CsPbBr_3$ overlapped more with the absorption spectra of Ag NPs when compared with other studied perovskites. Using the spectral integral, the overlap areas of 1.40, 3.70, and 9.90 were determined for the $CsPbI_3$, $CsPbBrI_2$, and $CsPbBr_3$, respectively. Since the overlap integral in the case of $CsPbBr_3$ is significantly higher, therefore, we expect the non-radiative energy transfer from $CsPbBr_3$ to the NPs, hence quenching is observed. A schematic of energy transfer quenching is shown in Fig. 10. However, in the case of $CsPbBrI_2$ and $CsPbI_3$, the overlap integral is less, and, therefore, energy is transferred from NPs to perovskite, increasing the excitation cross-section, which leads to PL enhancement (Fig. 11). [48]

However, PL enhancements were also observed for $CbPbBrI_2$ and $CsPbI_3$ perovskites at 570 nm and 620 nm (away from surface plasmon maximum of Ag NPs). The observed PL enhancements in these systems can be explained as follows. As shown in Fig. 9, it can be observed that the absorption of Ag nanoparticles extends all the way till 700 nm, which suggests that the plasmonic absorption is arising just not from spherical Ag NPs alone but also has a significant contribution from different size, shaped Ag Nanoparticles (inhomogeneity in sizes and shapes are quite common in ion-implanted nanomaterials). If the nanoparticles are completely spherical, one should absorb no absorption beyond 500 nm.[49] As the plasmonic absorption is extended till 700 nm in the present case, it is possible to observe plasmonic PL enhancement till that wavelength region although to a smaller extent than at 420 nm. Thus, even at excitation wavelengths of 570 nm for $CsPbBrI_2$

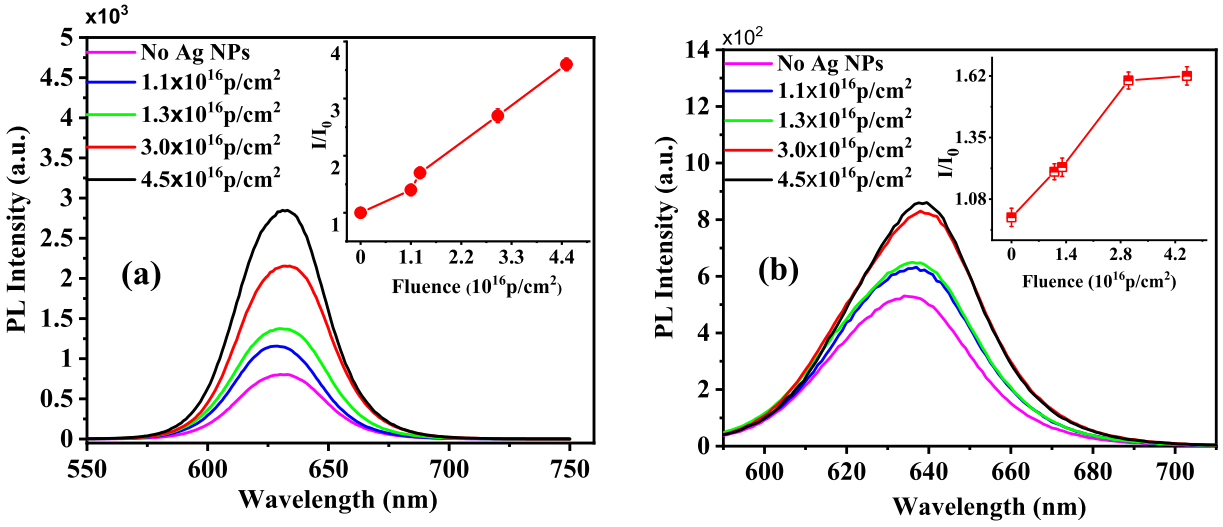

Fig. 6. PL intensity of $CsPbBrI_2$ perovskite on reference and Ag implanted quartz substrates after exciting at (a) 420 nm, and (b) 570 nm. The inset represents the corresponding PL enhancement factors.

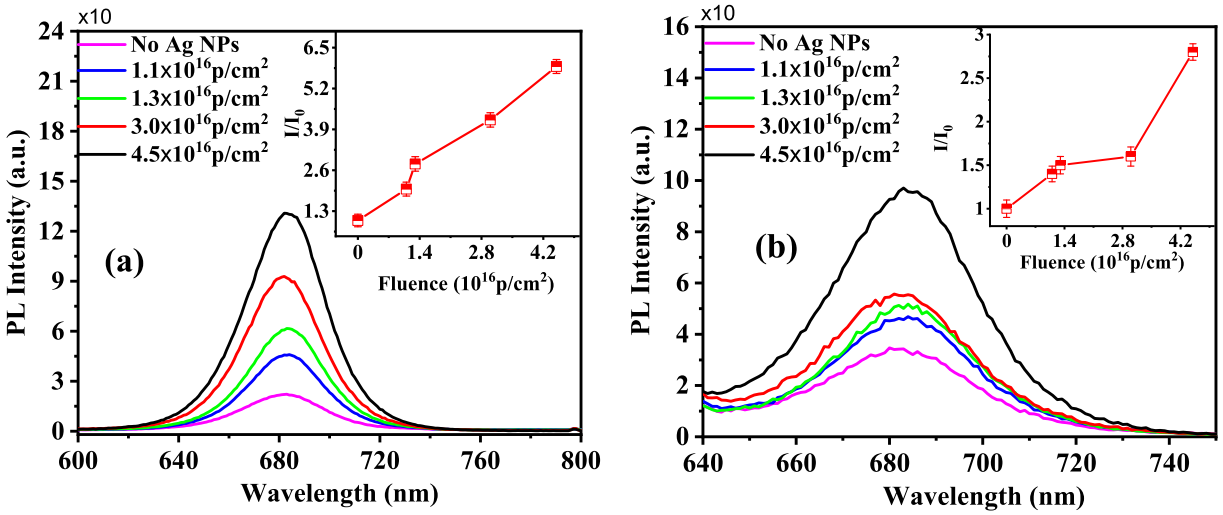

Fig. 7. PL intensity of $CsPbI_3$ perovskite on reference and Ag implanted quartz substrates after exciting at (a) 420 nm, and (b) 620 nm. The inset represents the corresponding PL enhancement factors.

Table 2
PL enhancement factor of $CsPbBrI_2$ and $CsPbI_3$ perovskite at different wavelengths and fluences.

Ion fluence (10^{16}p/cm^2)	$\frac{I}{I_0}$ of $CsPbBrI_2$ at 420 nm excitation	$\frac{I}{I_0}$ of $CsPbBrI_2$ at 570 nm excitation	$\frac{I}{I_0}$ of $CsPbI_3$ at 420 nm excitation	$\frac{I}{I_0}$ of $CsPbI_3$ at 620 nm excitation
1.1	1.4 ± 0.10	1.20 ± 0.03	2.0 ± 0.22	1.4 ± 0.10
1.3	1.7 ± 0.10	1.30 ± 0.04	2.8 ± 0.24	1.5 ± 0.15
3.0	2.7 ± 0.12	1.60 ± 0.03	4.2 ± 0.23	1.6 ± 0.10
4.5	3.6 ± 0.11	1.62 ± 0.04	5.9 ± 0.22	2.8 ± 0.12

and at 620 nm for $CsPbI_3$, contributions of plasmonic electric field enhancement from the ion-implanted Ag NPs is observed and resulted in the PL enhancement although the enhancement observed is smaller than the one at 420 nm. The question remains why the enhancement is more for $CsPbI_3$ at 620 nm when compared to $CsPbBrI_2$ at 570 nm and 620 nm excitation wavelengths. A closer look at the plasmonic absorption of Ag NPs (Fig. 9) reveals that the absorbance at 570 nm is only marginally higher compared to absorbance at 620 nm. On the other hand, there is a decent overlap of PL emission of $CsPbBrI_2$ with the absorption of Ag NPs when compared to $CsPbI_3$, leading to PL quenching. In such a scenario, smaller PL quenching for $CsPbI_3$ is expected, and that makes it to have greater PL enhancement when compared to $CsPbBrI_2$ at these off-resonance wavelengths. Note similar increased PL enhancement was observed for $CsPbI_3$ when compared to $CsPbBrI_2$ even at 420 nm.

4. Conclusions

Implanted Ag NPs were used to probe metal enhanced PL of perovskite nanocomposites. Implanted Ag NPs were synthesized using low energy ion implantation at different fluences. Implantation was carried out with Ag- ions and 70 keV ion beam energy and different fluences in quartz substrates. Optical absorption measurements have detected LSPR peaks of Ag NPs that confirm the formation of Ag NPs. An increase as well as redshift in the absorption peaks of Ag NPs was observed, which showed an increase in the size distribution of Ag NPs and the formation of hotspots. RBS measurements provided the depth profile of formed Ag NPs below the surface quartz substrates. RBS data revealed that nucleation of nanoparticles during the implantation process forces them closer to the substrate surface. Steady-state excitation and emission measurements were used to study metal enhanced PL of perovskites. PL quenching was observed in the case of $CsPbBr_3$ by silver nanoparticles

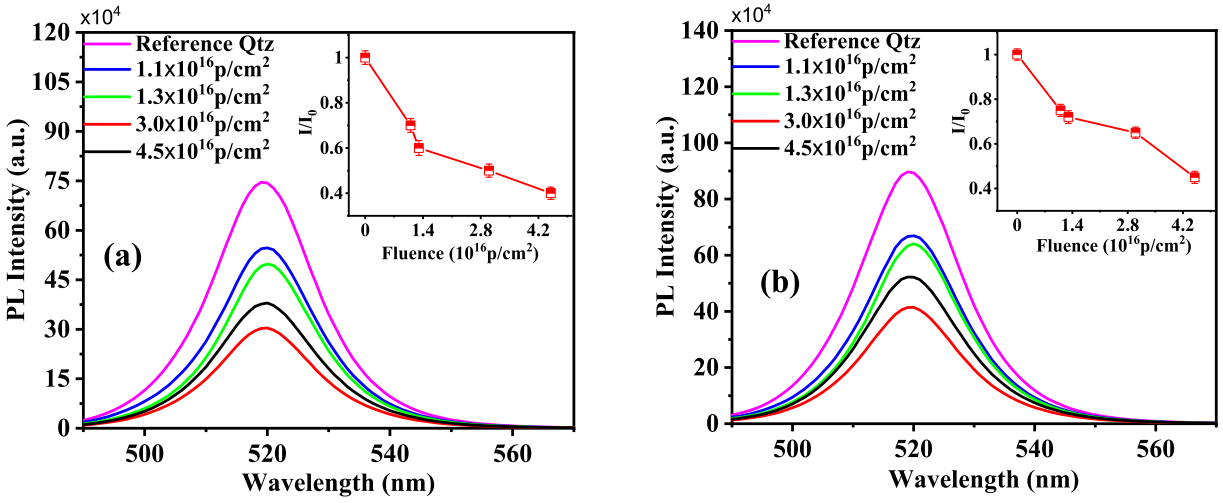

Fig. 8. PL intensity of $CsPbBr_3$ perovskite on reference and silver implanted quartz substrates after exciting at (a) 420 nm, and (b) 480 nm. Insets represent the corresponding PL quenching factors.

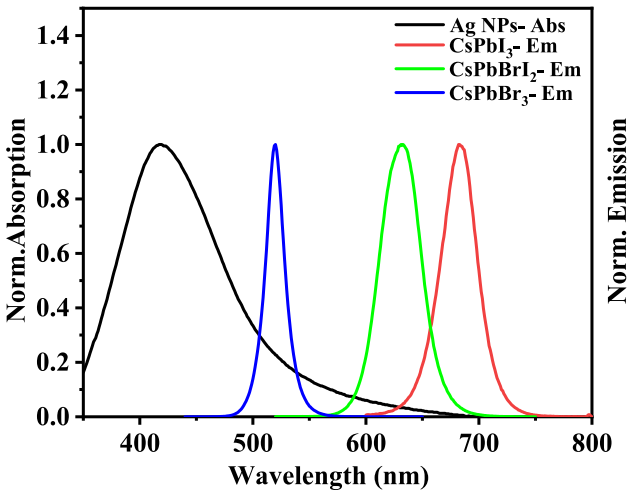

Fig. 9. Normalized emission and absorption spectra of perovskites and Ag NPs.

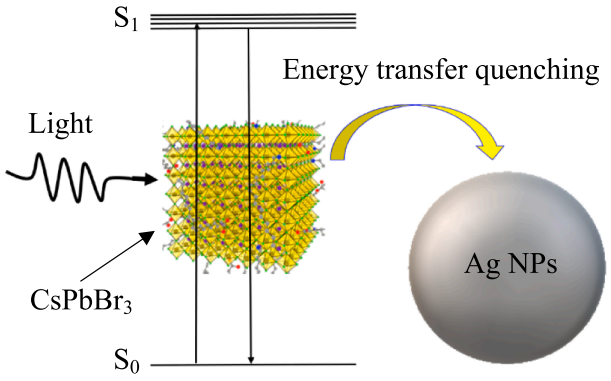

Fig. 10. Schematics of non radiative energy transfer from $CsPbBr_3$ to Ag NPs.

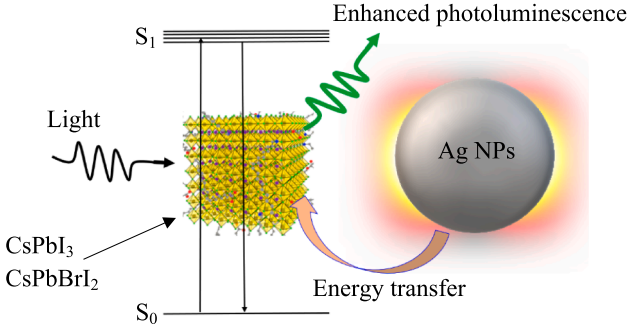

Fig. 11. Schematics of electromagnetic energy transfer from Ag NPs to perovskite nanocomposites.

that was attributed to the non-radiative energy transfer from $CsPbBr_3$ to Ag NPs. On other hand, enhanced PL of $CsPbI_3$ and $CsPbBrI_2$ was observed with maximum emission enhancement factors of 3.6 and 5.9. The PL enhancement factor was highest for the substrates implanted with high fluence. We conclude the PL enhancement was due to the enhanced electric field around NPs and the creation of hotspots. Moreover, PL enhancement also depends upon the excitation wavelength and integral overlapping of NPs absorption and CsPbX emission spectra. Excitation wavelength at LSPR peak produced max enhancement.

Declaration of Competing Interest

The authors declare that they have no known competing financial interests or personal relationships that could have appeared to influence the work reported in this paper.

Acknowledgments

The ion sources used in this project were purchased from NSF Grant ID: 1828387; and student support was provided by the Department of Physics at WMU. We acknowledge tremendous help received from WMU staff, Mr. Allan Kern, Mr. Benjamin Gaudio, Mr. Josh Byers, Mr. Rick Welch, Ms. Lori Krum and Ms. Robbin Dehaan.

References

[1] V.A.G. Rivera, F.A. Ferri, E. Marega, Localized Surface Plasmon Resonances: Noble Metal Nanoparticle Interaction with Rare-Earth Ions, in: Plasmon. - Princ. Appl., InTech, 2012. https://doi.org/10.5772/50753.
[2] Y.-T. Long, C. Jing, Localized surface plasmon resonance based nanobiosensors, springer, berlin heidelberg, berlin, Heidelberg (2014), https://doi.org/10.1007/978-3-642-54795-9.
[3] M. Singh, J. Truong, W. Reeves, J. Hahm, Emerging cytokine biosensors with optical detection modalities and nanomaterial-enabled signal enhancement, Sensors 17 (2017) 428, https://doi.org/10.3390/s17020428.
[4] P.K. Jain, M.A. El-Sayed, Plasmonic coupling in noble metal nanostructures, Chem. Phys. Lett. 487 (2010) 153–164, https://doi.org/10.1016/j.cplett.2010.01.062.
[5] E. Martinsson, Nanoplasmonic sensing using metal nanoparticles, Linköping University Electronic Press (2014), https://doi.org/10.3384/diss.diva-111841.
[6] P.K. Jain, W. Huang, M.A. El-Sayed, On the universal scaling behavior of the distance decay of plasmon coupling in metal nanoparticle pairs: a plasmon ruler equation, Nano Lett. 7 (2007) 2080–2088, https://doi.org/10.1021/nl071008a.
[7] M. Shabaninezhad, G. Ramakrishna, Theoretical investigation of size, shape, and aspect ratio effect on the LSPR sensitivity of hollow-gold nanoshells, J. Chem. Phys. 150 (2019), https://doi.org/10.1063/1.5090885.
[8] H. Chen, X. Kou, Z. Yang, W. Ni, J. Wang, Shape- and size-dependent refractive index sensitivity of gold nanoparticles, Langmuir 24 (2008) 5233–5237, https://doi.org/10.1021/la800305j.
[9] J. Zhu, Y. Ren, Tuning the plasmon shift and local electric field distribution of gold nanodumbbell: the effect of surface curvature transition from positive to negative, Appl. Surf. Sci. 285 (2013) 649–656, https://doi.org/10.1016/j.apsusc.2013.08.106.
[10] P.K. Jain, S. Eustis, M.A. El-Sayed, Plasmon coupling in nanorod assemblies: optical absorption, discrete dipole approximation simulation, and exciton-coupling model, J. Phys. Chem. B 110 (2006) 18243–18253, https://doi.org/10.1021/jp063879z.
[11] M. Shabaninezhad, A. Abuhagr, N.A. Sakthivel, C. Kumara, A. Dass, K. Kwak, K. Pyo, D. Lee, G. Ramakrishna, Ultrafast electron dynamics in thiolate-protected plasmonic gold clusters : size and ligand effect, J. Phys. Chem. C 123 (2019) 13344–13353, https://doi.org/10.1021/acs.jpcc.9b01739.
[12] J.P. Kottmann, O.J.F. Martin, D.R. Smith, S. Schultz, Dramatic localized electromagnetic enhancement in plasmon resonant nanowires, Chem. Phys. Lett. 341 (2001) 1–6, https://doi.org/10.1016/S0009-2614(01)00171-3.
[13] X. Zhang, Z. Zhao, L. Liu, Y. Li, Design of Gold nanorods Janus membrane for efficient and high-sensitive surface-enhanced Raman scattering and tunable surface plasmon resonance, Chem. Phys. Lett. 721 (2019) 117–122, https://doi.org/10.1016/j.cplett.2019.02.035.
[14] A. Kinkhabwala, Z. Yu, S. Fan, Y. Avlasevich, K. Müllen, W.E. Moerner, Large single-molecule fluorescence enhancements produced by a bowtie nanoantenna, Nat. Photonics 3 (2009) 654–657, https://doi.org/10.1038/nphoton.2009.187.
[15] S. Iqbal, M. Shabaninezhad, M. Hatshan, P.M. Niraula, A. Abuhagr, H. Alali, R. Guda, A. Kayani, Ion-implanted silver nanoparticles for metal-enhanced fluorescence, AIP Adv. 8 (2018), 095217, https://doi.org/10.1063/1.5045570.
[16] J.N. Anker, W.P. Hall, O. Lyandres, N.C. Shah, J. Zhao, R.P. Van Duyne, Biosensing with plasmonic nanosensors, Nat. Mater. 7 (2008) 442–453, https://doi.org/10.1038/nmat2162.
[17] J.R. Mejía-Salazar, O.N. Oliveira, Plasmonic Biosensing, Chem. Rev. 118 (2018) 10617–10625, https://doi.org/10.1021/acs.chemrev.8b00359.
[18] I.H. El-Sayed, X. Huang, M.A. El-Sayed, Surface Plasmon Resonance Scattering and Absorption of anti-EGFR Antibody Conjugated Gold Nanoparticles in Cancer Diagnostics: Applications in Oral Cancer, Nano Lett. 5 (2005) 829–834, https://doi.org/10.1021/nl050074e.
[19] P.K. Jain, X. Huang, I.H. El-Sayed, M.A. El-Sayed, Noble Metals on the Nanoscale: Optical and Photothermal Properties and Some Applications in Imaging, Sensing, Biology, and Medicine, Acc. Chem. Res. 41 (2008) 1578–1586, https://doi.org/10.1021/ar7002804.
[20] W. Deng, F. Xie, H.T.M.C.M. Baltar, E.M. Goldys, Metal-enhanced fluorescence in the life sciences: here, now and beyond, PCCP 15 (2013) 15695–15708, https://doi.org/10.1039/c3cp50206f.

[21] D. Darvill, A. Centeno, F. Xie, Plasmonic fluorescence enhancement by metal nanostructures: shaping the future of bionanotechnology, PCCP 15 (2013) 15709, https://doi.org/10.1039/c3cp50415h.
[22] P. Docampo, T. Bein, A Long-Term View on Perovskite Optoelectronics, Acc. Chem. Res. 49 (2016) 339–346, https://doi.org/10.1021/acs.accounts.5b00465.
[23] S.D. Stranks, H.J. Snaith, Metal-halide perovskites for photovoltaic and light-emitting devices, Nat. Nanotechnol. (2015), https://doi.org/10.1038/nnano.2015.90.
[24] S.A. Veldhuis, P.P. Boix, N. Yantara, M. Li, T.C. Sum, N. Mathews, S.G. Mhaisalkar, Perovskite Materials for Light-Emitting Diodes and Lasers, Adv. Mater. 28 (2016) 6804–6834, https://doi.org/10.1002/adma.201600669.
[25] X. Zhang, B. Xu, W. Wang, S. Liu, Y. Zheng, S. Chen, K. Wang, X.W. Sun, Plasmonic Perovskite Light-Emitting Diodes Based on the Ag–CsPbBr 3 System, ACS Appl. Mater. Interfaces 9 (2017) 4926–4931, https://doi.org/10.1021/acsami.6b12450.
[26] X. Wu, Y. Li, L. Wu, B. Fu, G. Liu, D. Zhang, J. Zhao, P. Chen, L. Liu, Enhancing perovskite film fluorescence by simultaneous near- and far-field effects of gold nanoparticles, RSC Adv. 7 (2017) 35752–35756, https://doi.org/10.1039/C7RA06744E.
[27] G. Xing, N. Mathews, S.S. Lim, N. Yantara, X. Liu, D. Sabba, M. Grätzel, S. Mhaisalkar, T.C. Sum, Low-temperature solution-processed wavelength-tunable perovskites for lasing, Nat. Mater. 13 (2014) 476–480, https://doi.org/10.1038/nmat3911.
[28] P. Sun, W.-W. Yu, X.-H. Pan, W. Wei, Y. Sun, N.-Y. Yuan, J.-N. Ding, W.-C. Zhao, X. Chen, N. Dai, Fluorescence Enhancement of Metal-Capped Perovskite CH 3 NH 3 PbI 3 Thin Films, Chinese Phys. Lett. 34 (2017), 096801, https://doi.org/10.1088/0256-307X/34/9/096801.
[29] F. Ren, X.H. Xiao, G.X. Cai, J.B. Wang, C.Z. Jiang, Engineering embedded metal nanoparticles with ion beam technology, Appl. Phys. A 96 (2009) 317–325, https://doi.org/10.1007/s00339-009-5205-3.
[30] U. Pal, O. Pea, Ion Implantation for the Fabrication of Plasmonic Nanocomposites: A Brief Review, in: Ion Implant., InTech, 2012. https://doi.org/10.5772/34397.
[31] L. Protesescu, S. Yakunin, M.I. Bodnarchuk, F. Krieg, R. Caputo, C.H. Hendon, R. X. Yang, A. Walsh, M.V. Kovalenko, Nanocrystals of Cesium Lead Halide Perovskites (CsPbX3, X = Cl, Br, and I): Novel Optoelectronic Materials Showing Bright Emission with Wide Color Gamut, Nano Lett. (2015), https://doi.org/10.1021/nl5048779.
[32] J.F. Ziegler, M.D. Ziegler, J.P. Biersack, SRIM – The stopping and range of ions in matter, Nucl. Instruments Methods Phys. Res. Sect. B Beam Interact. with Mater. Atoms. 268 (2010) 1818–1823. https://doi.org/10.1016/j.nimb.2010.02.091.
[33] M. Mayer, Improved physics in SIMNRA 7, Nucl. Instruments Methods Phys. Res. Sect. B Beam Interact. with Mater. Atoms. 332 (2014) 176–180, https://doi.org/10.1016/j.nimb.2014.02.056.
[34] A.L. Stepanov, Optical properties of metal nanoparticles synthesized in a polymer by ion implantation: A review, Tech. Phys. 49 (2004) 143–153, https://doi.org/10.1134/1.1648948.
[35] A.L. Stepanov, Synthesis of silver nanoparticles in dielectric matrix by ion implantation: A review, Rev. Adv. Mater. Sci. 26 (2010) 1–29.
[36] P. Sun, W.W. Yu, X.H. Pan, W. Wei, Y. Sun, N.Y. Yuan, J.N. Ding, W.C. Zhao, X. Chen, N. Dai, Fluorescence Enhancement of Metal-Capped Perovskite CH3NH3PbI3 Thin Films, Chinese Phys. Lett. (2017), https://doi.org/10.1088/0256-307X/34/9/096801.
[37] E. Thune, T. Cabioc'h, P. Guérin, M.-F. Denanot, M. Jaouen, Nucleation and growth of carbon onions synthesized by ion-implantation: a transmission electron microscopy study, Mater. Lett. 54 (2002) 222–228. https://doi.org/10.1016/S0167-577X(01)00567-5.
[38] T. Ming, L. Zhao, Z. Yang, H. Chen, L. Sun, J. Wang, C. Yan, Strong polarization dependence of plasmon-enhanced fluorescence on single gold nanorods, Nano Lett. 9 (2009) 3896–3903, https://doi.org/10.1021/nl902095q.
[39] Q. Hao, D. Du, C. Wang, W. Li, H. Huang, J. Li, T. Qiu, P.K. Chu, Plasmon-induced broadband fluorescence enhancement on Al-Ag bimetallic substrates, Sci. Rep. 4 (2015) 6014, https://doi.org/10.1038/srep06014.
[40] M. Bayle, C. Bonafos, P. Benzo, G. Benassayag, B. Pécassou, L. Khomenkova, F. Gourbilleau, R. Carles, Ag doped silicon nitride nanocomposites for embedded plasmonics, Appl. Phys. Lett. 107 (2015), 101907, https://doi.org/10.1063/1.4930940.
[41] C. Farcau, C. Bonafos, P. Benzo, G. Benassayag, R. Carles, Combining elastic and resonant inelastic optical spectroscopies for multiscale probing of embedded nanoparticle architectures, J. Appl. Phys. 108 (2010), https://doi.org/10.1063/1.3506680.
[42] A. Stepanov, V. Popok, Nanosecond pulse laser and furnace annealing of silver nanoparticles formed by implantation in silicate glass, Surf. Coatings Technol. 185 (2004) 30–37, https://doi.org/10.1016/j.surfcoat.2003.11.025.
[43] A.L. Stepanov, D.E. Hole, P.D. Townsend, Modification of size distribution of ion implanted silver nanoparticles in sodium silicate glass using laser and thermal annealing, Nucl. Instruments Methods Phys. Res. Sect. B Beam Interact. with Mater. Atoms. 149 (1999) 89–98, https://doi.org/10.1016/S0168-583X(98)90733-9.
[44] A.L. Stepanov, Nonlinear optical properties of implanted metal nanoparticles in various transparent matrixes NONLINEAR OPTICAL PROPERTIES OF IMPLANTED METAL NANOPARTICLES IN VARIOUS TRANSPARENT MATRIXES: A REVIEW, Rev. Adv. Mater. Sci. (2011).
[45] Q. Fu, W. Sun, Mie theory for light scattering by a spherical particle in an absorbing medium, Appl. Opt. 40 (2001) 1354, https://doi.org/10.1364/AO.40.001354.
[46] Y.-P. Hsieh, C.-T. Liang, Y.-F. Chen, C.-W. Lai, P.-T. Chou, Mechanism of giant enhancement of light emission from Au/CdSe nanocomposites, Nanotechnology. 18 (2007), 415707, https://doi.org/10.1088/0957-4484/18/41/415707.
[47] S.T. Kochuveedu, D.H. Kim, Surface plasmon resonance mediated photoluminescence properties of nanostructured multicomponent fluorophore systems, Nanoscale. 6 (2014) 4966–4984, https://doi.org/10.1039/C4NR00241E.
[48] N. Shemeena Basheer, B. Rajesh Kumar, A. Kurian, S.D. George, Thermal lens probing of distant dependent fluorescence quenching of Rhodamine 6G by silver nanoparticles, J. Lumin. 137 (2013) 225–229, https://doi.org/10.1016/j.jlumin.2012.12.052.
[49] E. Hao, G.C. Schatz, Electromagnetic fields around silver nanoparticles and dimers, J. Chem. Phys. 120 (2004) 357–366, https://doi.org/10.1063/1.1629280.